




Article

Improvement of Peptidyl Copper Complexes Mimicking Catalase: A Subtle Balance between Thermodynamic Stability and Resistance towards H₂O₂ Degradation

Yaqine Ben Hadj Hammouda ^{1,2,†}, Koudedja Coulibaly ^{1,†} , Alimatou Bathily ¹, Magdalene Teoh Sook Han ¹, Clotilde Policar ¹  and Nicolas Delsuc ^{1,*} 

¹ Laboratoire des Biomolécules, LBM, Département de Chimie, Ecole Normale Supérieure, PSL University, Sorbonne Université, CNRS, 75005 Paris, France

² Département de Chimie, Ecole Normale Supérieure, PSL University, 75005 Paris, France

* Correspondence: nicolas.delsuc@ens.psl.eu

† These authors contributed equally to this work.

Abstract: Catalase mimics are low molecular weight metal complexes that reproduce the activity of catalase, an antioxidant metalloprotein that participates in the cellular regulation of H₂O₂ concentration by catalyzing its dismutation. H₂O₂ is a reactive oxygen species that is vital for the normal functioning of cells. However, its overproduction contributes to oxidative stress, which damages cells. Owing to their biocompatibility, peptidyl complexes are an attractive option for clinical applications to regulate H₂O₂ by enzyme mimics. We report here the synthesis and characterization of four new peptidyl di-copper complexes bearing two coordinating sequences. Characterization of the complexes showed that, depending on the linker used between the two coordinating sequences, their catalytic activity for H₂O₂ dismutation, their thermodynamic stability and their resistance to H₂O₂ degradation are very different, with (CATm2)Cu₂ being the most promising catalyst.

Keywords: catalase mimic; di-copper(II) complexes; H₂O₂ dismutation; metal binding peptide; reactive oxygen species



Citation: Ben Hadj Hammouda, Y.; Coulibaly, K.; Bathily, A.; Teoh Sook Han, M.; Policar, C.; Delsuc, N. Improvement of Peptidyl Copper Complexes Mimicking Catalase: A Subtle Balance between Thermodynamic Stability and Resistance towards H₂O₂ Degradation. *Molecules* **2022**, *27*, 5476. <https://doi.org/10.3390/molecules27175476>

Received: 19 July 2022

Accepted: 22 August 2022

Published: 26 August 2022

Publisher's Note: MDPI stays neutral with regard to jurisdictional claims in published maps and institutional affiliations.

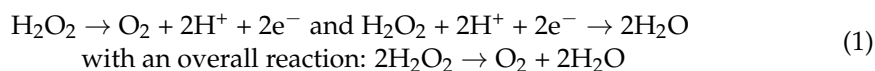


Copyright: © 2022 by the authors. Licensee MDPI, Basel, Switzerland. This article is an open access article distributed under the terms and conditions of the Creative Commons Attribution (CC BY) license (<https://creativecommons.org/licenses/by/4.0/>).

1. Introduction

Reactive oxygen species (ROS) such as superoxide anion O₂^{•−} or hydrogen peroxide H₂O₂ are by-products of the respiratory chain in aerobic organisms. Though essential for fundamental cellular mechanisms such as signalization, an excess of these species leads to oxidative stress and may cause damage to the cells [1–5]. Thus, their intracellular level is tightly controlled by antioxidant defenses, which include metalloenzymes such as superoxide dismutase (SOD) and catalase (CAT). SODs catalyze the dismutation of O₂^{•−} through a one-electron exchange process, forming O₂ and H₂O₂ [6–8]. H₂O₂ concentration is regulated by CAT or glutathione peroxidase [9,10]. H₂O₂ is better tolerated in cells than superoxide (nM to low μM, whereas steady superoxide concentration is in the pM range) [11] and HO[•], which is the most reactive of the three, with a cellular half-life in the ns range [12]. However, H₂O₂ can be easily transformed into the most damaging HO[•] by reacting with intracellular copper (I) complexes or iron through the Fenton reaction. Therefore, the development of CAT mimics that could complement CAT when these enzymes are overwhelmed may contribute to oxidative stress management. While SOD mimics have been extensively studied as potential catalytic therapeutic molecules [13–16], the exploration of CAT mimics is still in its infancy [17–19]. On the one hand, some mononuclear manganese mimics have been tested in cellular models, but they lacked stability in such intricate environments [17]. On the other hand, iron or manganese porphyrins, which are much more stable, have shown beneficial effects on H₂O₂-mediated loss of viability in catalase/peroxidase-deficient *E. coli* strains [18]. Finally, a di-copper peptidyl catalase

mimic has shown the ability to reduce H₂O₂ concentration in HeLa Hyper cells [19]. There are two types of catalases: a (monometallic) heme CAT [20] and a dinuclear manganese CAT [21], present in bacteria such as *Lactobacillus plantarum* [22]. Unlike O₂^{•−}, H₂O₂ dismutation by CAT requires two electrons, following the half-reactions:



Therefore, CAT mimics need to be bi-electronic as well. So far, the majority of bioinspired mimics have been mononuclear Fe or Mn porphyrinic complexes [18,23], with the ligand porphyrin being easily oxidizable and participating in the bi-electronic exchange, and di-nuclear non-heme Mn complexes [17,24]. A few examples of nanoparticles and metal–organic framework (MOF) nanoparticles have also been identified as CAT mimics [25,26], as well as a few copper complexes [27–32]. However, their catalytic activity was often reported in organic solvents or at non-physiological pH because of their low solubility in aqueous pH 7.5 conditions or the need for an external base. We recently described the first peptidyl di-copper complex with catalase-like activity that was promising in aqueous buffer and in cells [19]. However, its first-order rate for H₂O₂ dismutation, k_{cat} , was still two orders of magnitude smaller than that of most active reported non-peptidyl mimics [18]. In addition, we showed that the complex was rapidly degraded in the presence of H₂O₂. Herein, we report a second generation of rationally designed copper peptidyl complexes with enhanced stability and a better affinity for copper, especially on the lowest-affinity binding site. Herein, we describe four new complexes. There is a subtle balance between complexes' thermodynamic stability, their catalytic activity and their ability to resist H₂O₂ degradation. Indeed, a complex with high intrinsic catalytic activity will not be able to react with H₂O₂ molecules if it is degraded too quickly. On the other hand, if it shows great thermodynamic stability with Cu(II), which prefers square planar geometries, it may not be able to perform electron transfer or to accommodate Cu(I), which prefers tetrahedral geometry, and/or bind to H₂O₂ molecules. In such situations, its catalase-like activity will be low. The four new complexes displayed catalase-like activity, and, very interestingly, some of them showed improved features, such as higher resistance to H₂O₂ degradation and greater thermodynamic stability in comparison with the previously described peptidyl copper complex [19].

2. Results and Discussion

2.1. Design and Synthesis

The screening of a combinatorial library of peptidyl copper(II) complexes combined with a catalase activity-based assay enabled the identification of the first peptidyl di-copper complex with promising CAT activity [19]. This first peptide, called CATm1, is shown in Table 1. Its in-depth study confirmed the desired stoichiometry of one peptide for two copper(II) ions to enable two-electron transfer. EPR characterization of the resulting complex suggested a square planar geometry with an N4 or N3O ligand coordination site around both copper atoms, and fluorescence titration revealed two coordination sites with ${}^{\text{app}}K_{d1} = 2.8 \pm 0.6 \times 10^{-6}$ and ${}^{\text{app}}K_{d2} = 8.5 \pm 4.9 \times 10^{-6}$ for the first and second sites, respectively. Moreover, despite promising catalytic activity, the first-order rate of H₂O₂ dismutation, k_{cat} , was still two orders of magnitude smaller than that of most manganese non-peptidyl mimics [18]. In addition, the complex undergoes fast degradation in the presence of H₂O₂. Therefore, these results invited the improvement of the overall stability of the complex, especially on the second coordination site.

To do so, a second generation of peptides was rationally designed with two repetitions of the supposed first binding site, PHYKH, which has a higher affinity for copper (II), without (CATm2) or with a spacer (CATm3, CATm4 and CATm5). As spacers, one (CATm3) or two glycine residues (CATm4 and CATm5) were introduced (see Table 1). The introduction of the glycine linker, leading to a glycine–proline (GP) motif (in CATm3 and CATm4), may favor a turn conformation within the peptide chain [33]. Consequently, in

CATm5, the proline residue was removed to possibly evaluate the influence of this turn conformation on the resulting copper complex properties.

Table 1. Sequence of the peptidyl ligands studied. In bold are highlighted residues that may favor a turn conformation.

Name	Peptide Sequence
CATm1	Ac(PHYKH)RLH-NH ₂
CATm2	Ac(PHYKH)(PHYKH)-NH ₂
CATm3	Ac(PHYKH) G (PHYKH)-NH ₂
CATm4	Ac(PHYKH) GG (PHYKH)-NH ₂
CATm5	Ac(PHYKH)GGHYKH-NH ₂

The peptides were synthesized by solid-phase peptide synthesis (SPPS) on rink amide resin using a Fmoc strategy. The coupling steps were performed using *N,N'*-diisopropylcarbodiimide (DIC) and 1-hydroxybenzotriazole (HOBt) as coupling agents. Fmoc deprotection was achieved using a solution of piperidine in DMF (20:80 *v:v*). Each step was monitored using a colorimetric assay (the Kaiser test). After acetylation of the N-terminus, the peptides were cleaved using a TFA solution containing H₂O and triisopropylsilane (95:2.5:2.5 *v:v:v*). The peptides were precipitated in cold diethyl ether, washed three times with neat diethyl ether and purified by reverse-phase HPLC. The pure peptides were identified by MALDI-TOF mass spectrometry (Figure S1 and Table S1 in Supplementary Materials).

2.2. Complexes' Thermodynamic Stability

One of the main challenges in improving catalyst efficiency is to gain thermodynamic stability of the complexes and, in particular, to enhance the second coordination site's affinity for copper. In order to gain insights into the stability of the complexes, titration was performed by fluorescence spectroscopy since the four new peptides contain two fluorescent tyrosine residues (Y), which can be excited at 275 nm and emit at 303 nm. The fluorescence of tyrosine was quenched when adding copper, possibly because it is one of the Cu(II) ligands. For each peptide, titrations were performed at least twice in MOPS buffer (50 mM, pH 7.5) in order to (i) confirm the 1:2 peptide:Cu(II) stoichiometry of the complex, as with CATm1, and (ii) determine the association constants of the two coordination sites. Titrations performed at high peptide concentration (ca. 72 μM) showed unambiguously that each peptide is able to coordinate two copper metal ions (Figure S2a). The curves obtained during titrations at lower concentrations (10–30 μM) could be fitted with a 1-to-2 peptide:Cu model using HypSpec software (Figure S2b–f). The values are reported in Table S2 and presented in Figure 1 for comparison.

The association constant for the first binding site underwent an increase of one to two orders of magnitude, except for CATm3, which decreased. The highest association constants were obtained with CATm2 and CATm5. On the other hand, the association constant of the second binding site slightly decreased with CATm3 and CATm4. As for the first binding site, the peptides CATm2 and CATm5 seemed to lead to complexes with a more stable second site. CATm2 has no linker between the two repeated sequences (PHYKH), and CATm5 has two glycines and no proline. Consequently, none of these peptides contains the GP sequence, which seems deleterious to achieving a stable second coordination site. The conformation of the peptides, as non-metalated ligand and copper(II) complexes, were further investigated by circular dichroism (CD). None of the ligands adopted a specific conformation (Figure S3), and all complexes exhibited a similar weak CD signature with two maxima at 230 and 260 nm, revealing a low degree of structuration upon binding. When the spectra were normalized according to the number of residues within each peptide, the spectrum of the (CATm1)Cu₂ complex showed the most intense bands (Figure 2). This suggests a higher content of a defined conformation for this complex in comparison with the others. However, since the higher intensity of these bands does not

correlate with higher affinity constants, this conformation may not be the conformation leading to the most stable complexes.

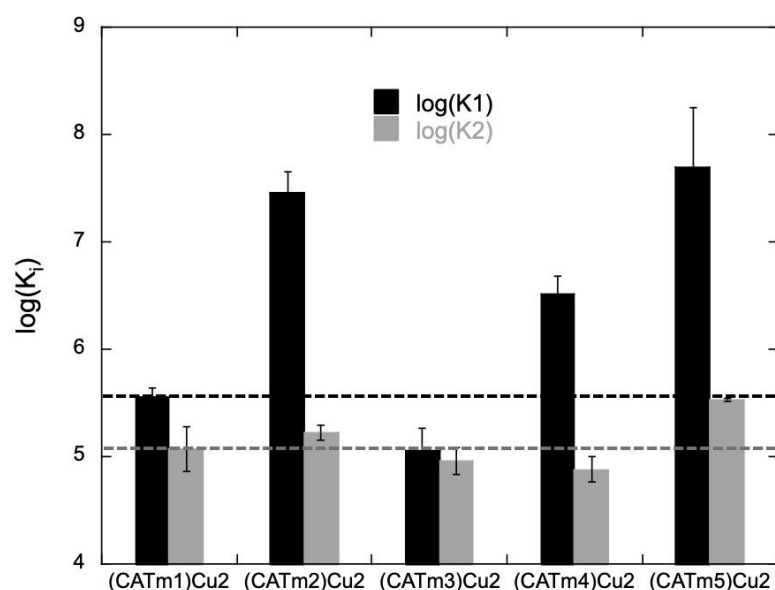


Figure 1. Comparison of $\log(^{app}K_1)$ and $\log(^{app}K_2)$ of the 1:2 peptide:Cu complexes. The apparent association constants of the two binding sites for each complex were measured using fluorescence spectroscopy at 25 °C in MOPS buffer (50 mM, pH 7.5) using HypSpec software. HypSpec determined cumulative (β) binding constants for the first (β_1) and second (β_2) Cu(II) bindings to the peptide. From these cumulative binding constants, the stepwise binding constants for the first (K1) and second (K2) Cu(II) bound to the peptide were determined. The provided ^{app}K values are the average of two to three independent titrations \pm standard error of the mean (SEM). Excitation was set at 275 nm, and spectra were recorded from 280 to 400 nm (see Experimental Section for more details).

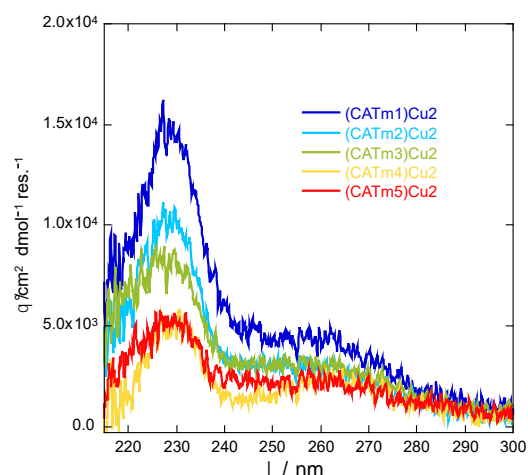


Figure 2. Circular dichroism spectra normalized by the number of residues within each peptide of CATmx:Cu 1:2 mixtures ($[CATmx] = 133 \mu M$, $x = 1-5$). Spectra were recorded at 20 °C in MOPS buffer (50 mM, pH 7.5).

2.3. Kinetic Study of Complex Degradation in the Presence of H₂O₂

Previous studies with the (CATm1)Cu₂ complex indicated its rapid degradation in the presence of H₂O₂ [19]. Thus, the new complexes were also investigated for their resistance to degradation by H₂O₂. It was shown for (CATm1)Cu₂ that, in a large excess of H₂O₂, the complex is transformed into products with a characteristic absorption band at 289 nm. This most likely results from the modification of the phenol ring of the tyrosine. Notably, this is not the case for the non-metalated ligand or Cu(OAc)₂ [19]. Similar degradation products

were obtained with the newly developed complexes, with UV-vis spectra differing only by the intensities of the absorption maxima (Figure S4). We investigated the degradation kinetics of all complexes to better assess their resistance under catalytic conditions. The formation rate of the degradation products can be written as follows:

$$v_0 = k_{cat}[\text{H}_2\text{O}_2]_0[\text{catalyst}]_0 \quad (2)$$

or as

$$v_0 = k_{obs}[\text{catalyst}]_0 \quad (3)$$

under pseudo-first-order conditions by using a large excess of H_2O_2 during the experiments. Measuring the initial rate at different complex concentrations (20, 50, 100 and 200 μM) enabled the determination of the apparent kinetic constant k_{obs} (Figure 3 and Table 2). In this experiment, a low k_{obs} indicates a high resistance to H_2O_2 degradation.

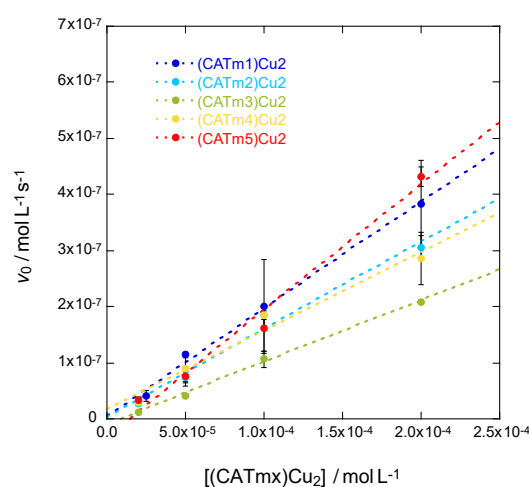


Figure 3. Determination by UV-vis spectrometry at 289 nm of the apparent kinetic constants of degradation product formation for complexes $(\text{CATm}x)\text{Cu}_2$ ($x = 1$ to 5) in MOPS (50 mM, pH 7.5) with an excess of H_2O_2 (5 mM).

Table 2. Rates of catalyst degradation under pseudo-first-order conditions ($[\text{H}_2\text{O}_2] = 5$ mM) at 25 °C in MOPS buffer (50 mM, pH 7.5) obtained from the slopes of the lines in Figure 3.

	k_{obs} (s^{-1})
$(\text{CATm}1)\text{Cu}_2$ ^a	1.90×10^{-3}
$(\text{CATm}2)\text{Cu}_2$	1.56×10^{-3}
$(\text{CATm}3)\text{Cu}_2$	1.10×10^{-3}
$(\text{CATm}4)\text{Cu}_2$	1.41×10^{-3}
$(\text{CATm}5)\text{Cu}_2$	2.24×10^{-3}

^a The value is different from the value reported in Reference [19] because the extinction coefficient was measured differently (see Supporting Information for more details about extinction coefficient determination and Figure S6).

The complexes $(\text{CATm}2)\text{Cu}_2$, $(\text{CATm}3)\text{Cu}_2$ and $(\text{CATm}4)\text{Cu}_2$ exhibited a smaller k_{obs} than $(\text{CATm}1)\text{Cu}_2$, meaning their degradation is slower. On the other hand, $(\text{CATm}5)\text{Cu}_2$ degradation was faster than $(\text{CATm}1)\text{Cu}_2$ degradation. The overall order of degradation, from the slowest to the fastest, is $(\text{CATm}3)\text{Cu}_2 < (\text{CATm}4)\text{Cu}_2 < (\text{CATm}2)\text{Cu}_2 < (\text{CATm}1)\text{Cu}_2 < (\text{CATm}5)\text{Cu}_2$. This does not correlate with the thermodynamic stability of the complexes, suggesting that the degradation of the complexes may not be due to released Cu(I) that could have reacted with H_2O_2 to form radicals such as HO^\bullet . Indeed, the complexes' degradation may also result from a reaction with HO^\bullet , which is generated by the complexes themselves, as has been described for amyloid peptide/Cu complexes [34].

2.4. Catalytic Activity

The ability of the four complexes to catalyze hydrogen peroxide dismutation and to thus mimic the enzyme CAT was then investigated. A Clark-type electrode can be used to monitor O_2 formation when H_2O_2 is added to the complex solution (see Figure S5 for representative experiments). The catalase activity of many complexes mimicking CAT has only been studied in organic solvents or at relatively high pH [29,32,35], except for a few [31,35–37]. With peptidyl complexes, aqueous solubility at pH around 7 allowed us to conduct studies in more biologically relevant conditions, namely, in aqueous MOPS buffer (50 mM) at pH 7.5. While the initial concentration of the complex $CAT_{mx}:Cu(OAc)_2$ 1:2 was held constant at 100 μM , the reaction was studied with variable amounts of H_2O_2 (from 2.5 mM to 30 mM). Endogenous MnCAT exhibits Michaelis–Menten catalytic behavior [38]. The initial rate of O_2 formation satisfies the Michaelis–Menten equation:

$$v_0 = \frac{v_{\max}[H_2O_2]_0}{K_M + [H_2O_2]_0} \quad (4)$$

where v_0 is the initial rate, v_{\max} is the maximum rate for a given catalyst concentration, K_M is the Michaelis–Menten constant and is a measure of the catalyst affinity for H_2O_2 (the lower the K_M , the higher the affinity), and $[H_2O_2]_0$ is the initial substrate concentration. We can also write:

$$v_{\max} = k_{\text{cat}}[\text{Catalyst}]_0 \quad (5)$$

with k_{cat} being the catalytic rate constant for H_2O_2 dismutation. These different catalytic parameters can be easily determined using the Lineweaver–Burk method involving the reciprocal of Equation (5):

$$\frac{1}{v_0} = \left(\frac{K_M}{v_{\max}} \right) \left(\frac{1}{[H_2O_2]_0} \right) + \frac{1}{v_{\max}} \quad (6)$$

When $1/v_0$ is plotted against $1/[H_2O_2]_0$, the slope of the obtained line gives K_M/v_{\max} , and the intercept with the x-axis (abscissa) gives $-1/K_M$. k_{cat} is then calculated according to Equation (5) (Figure 4a). Experiments were repeated at least twice to ensure the consistency of the results, which are summarized in Table 3.

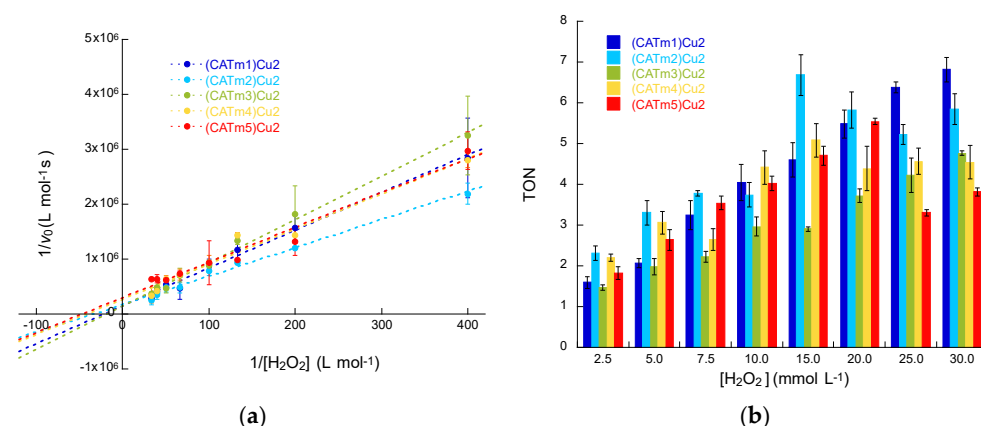


Figure 4. Catalytic behavior of the five $CAT_{mx}:Cu$ 1:2 complexes in MOPS (50 mM, pH 7.5) at 25 °C. Experiments were performed with $[(CAT_{mx})Cu_2] = 100 \mu M$ ($x = 1-5$). (a) Lineweaver–Burk plot (double reciprocal of the Michaelis–Menten equation), allowing the determination of enzyme kinetic parameters. (b) Turnover numbers (TONs) of dismutated H_2O_2 measured at various $[H_2O_2]$ concentrations. Data are given as the average of at least 2 experiments \pm standard error of the mean (SEM). Notably, kinetics values for $[(CAT_{m1})Cu_2]$ are slightly different from previously reported data [19] since, in this work, kinetics were measured in a larger $[H_2O_2]$ concentration range, which led to a different slope in Figure 4a.

Dismutation transforms 2 moles of H₂O₂ into 1 mole of O₂ (Equation (1)). Hence, the catalytic rate constant k_{cat} for H₂O₂ dismutation corresponds to 2^*k_{cat} for O₂ formation. All kinetic parameters reported hereafter are according to H₂O₂, even if it is O₂ evolution that was monitored. The results are reported in Table 3. The catalytic rates k_{cat} of the four new complexes are in the same order of magnitude as (CATm1)Cu₂. (CATm3)Cu₂ showed the best catalytic rate constant ($1.3 \times 10^{-1} \text{ s}^{-1}$) but also the weakest affinity for H₂O₂ ($K_M = 52 \text{ mM}$). In order to take into account these two features, the ratio k_{cat}/K_M , which better reflects catalytic efficiency, was calculated. CATm2 is the peptide leading to the most efficient complex since its k_{cat}/K_M ratio ($3.9 \text{ M}^{-1} \text{ s}^{-1}$) is the highest, followed by CATm5 ($3.2 \text{ M}^{-1} \text{ s}^{-1}$). Interestingly, these data are consistent with the thermodynamic constants measured by fluorescence since (CATm2)Cu₂ and (CATm5)Cu₂ are the most thermodynamically stable complexes (Figure 1). The apparent second-order constant (k_{cat}/K_M) for the 1:2 complexes is higher than the values reported for other copper(II) complexes, except for CuL₂ (Table 3).

Table 3. Parameters describing the catalysis of H₂O₂ dismutation.

	K_M (M)	k_{cat} (s ⁻¹)	k_{cat}/K_M (M ⁻¹ .s ⁻¹)	References
(CATm1)Cu ₂ [a]	4.8×10^{-2}	1.4×10^{-1}	2.9	This work, [19]
(CATm2)Cu ₂ [a]	2.9×10^{-2}	1.1×10^{-1}	3.9	This work
(CATm3)Cu ₂ [a]	5.2×10^{-2}	1.3×10^{-1}	2.5	This work
(CATm4)Cu ₂ [a]	2.4×10^{-2}	0.8×10^{-1}	3.1	This work
(CATm5)Cu ₂ [a]	2.1×10^{-2}	0.7×10^{-1}	3.2	This work
Cu(N-baa) ₂ (phen) [b]	5.2×10^{-2}	6.6×10^{-2}	1.3	[29]
[Cu(HL1)] ²⁺ [c]	1.7×10^1	1.5×10^{-3}	8.9×10^{-5}	[31]
Cu ₂ (pxdiprbtacn)Cl ₄ [d]	1.5	1.24	0.8	[36]
CuL ₂ [e]	4.2×10^{-2}	3.6×10^{-1}	8.25	[37]
[Cu(apzpn)] ²⁺ [f]			1.10	[35]
[Cu(py ₂ pn)] ²⁺ [g]		0.8×10^{-4}		[32]
Catalase	8.3×10^{-2}	2.6×10^5	3.1×10^6	[38]

[a] k_{cat} is the first-order rate of H₂O₂ dismutation, and K_M is the Michaelis–Menten constant. In this work, they were measured with the CATm1:Cu²⁺ 1:2 mixture at 100 μM. Reactions were performed in MOPS buffer (50 mM, pH 7.5) at 25 °C. [b] N-baaH: N-benzoylanthranilic acid; phen: 1,10-phenanthroline. The reactions were performed in DMF at 20 °C. [c] HL¹: 1,3-bis[(2-aminoethyl)amino]-2-propanol. The reactions were performed at 25 °C in TRIS buffer, pH 7. [d] pxdiprbtacn: 1,4-Bis(4,7-diisopropyl-1,4,7-triazacyclonon-1-ylmethyl)benzene. The reactions were performed in phosphate buffer (0.01 M, pH = 7.4) at 25 °C. [e] L²: 2-[[3-chloro-2-hydroxy-propyl]-pyridin-2-ylmethyl-amino]-methyl-phenol. The reactions were performed in phosphate buffer solution at pH 7.8. [f] apzpn: N,N'-bis(2-acetylpyrazyl)methylene-1,3-diaminopropane. The reactions were performed at 30.0 ± 0.1 °C in borate buffer (0.10 M, pH 8). [g] py₂pn: N,N'-Bis(2-pyridinylmethylene)propane-1,3-diamine. The reactions were performed at 25 °C in DMF solution of the complex containing 100 mM of Et₃N.

The overall efficiency of a CAT mimic must be evaluated while taking into account its reactivity towards H₂O₂ and its resistance to degradation. To that end, the turnover numbers (TONs) were calculated using the previous kinetic data (Figure 4b). The TON is the number of moles of converted substrate (H₂O₂) per mole of catalyst and gives an estimation of the longevity of a catalyst. For all complexes, the TON increased when H₂O₂ concentration increased to 7.5 mM, with (CATm2)Cu₂ always possessing the highest TON. This is consistent with its higher k_{cat}/K_M ratios. At 10 mM, the four catalysts (CATm1)Cu₂, (CATm2)Cu₂, (CATm4)Cu₂ and (CATm5)Cu₂ exhibited similar TON values, whereas the least efficient catalyst (CATm3)Cu₂ showed weaker TON values. At high H₂O₂ concentrations (25 and 30 mM), the TON value of (CATm5)Cu₂, the most fragile complex (according to the previous experiment; see Figure 3), dropped, whereas the TON value of

(CATm3)Cu₂, which is the more resistant complex to H₂O₂ degradation, kept increasing. This clearly shows that at these concentrations, the degradation of the catalyst becomes a key parameter. The TON values did not increase when the experiments were performed in the presence of D-mannitol, a HO• quencher (up to 1 mM, data not shown), suggesting that the complexes were not degraded because of HO• formation.

3. Conclusions

Ultimately, the overall efficacy of a complex as a CAT mimic depends on a fine balance between several parameters, including its reactivity towards H₂O₂; its own stability and affinity for its metal, determining its survival in biological conditions; and its resistance to H₂O₂ degradation, which remains a strong oxidant. In order to take into account all of these features, radar plots were used for comparison purposes (Figure 5). We chose to report the three main parameters that play an important role in the catalysis (thermodynamic stability, dismutation kinetics and resistance to degradation). The axes were chosen so that an increase was associated with an improvement: hence, we chose the overall stability of the complexes ($\log(K_{a1} \cdot K_{a2})$), the kinetics of the dismutation k_{cat}/K_M and the inverse of the degradation rate. In such radar plots, the higher the surface, the better the catalyst.

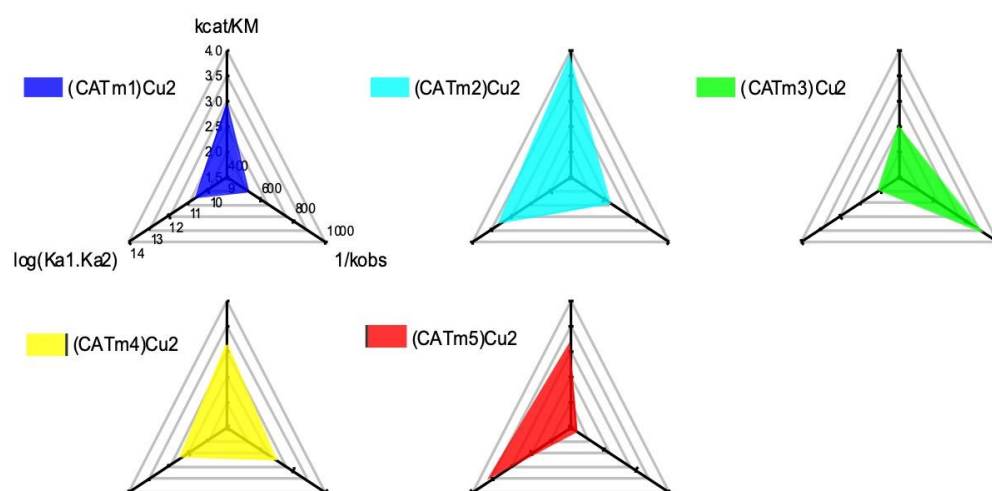


Figure 5. Comparison of catalyst performance using radar representation. k_{cat}/k_M are parameters related to the kinetics of H₂O₂ dismutation, K_{a1} and K_{a2} are the association constants of the two binding sites, and k_{obs} is the rate of degradation of the catalyst in the presence of an excess of H₂O₂.

Using such representations, it clearly appears that the area in the case of (CATm2)Cu₂ is the widest, indicating that this complex is the most promising catalyst. Interestingly, the CATm2 sequence is the shortest of the four new sequences investigated, suggesting that compact structures may be more suitable for developing efficient catalysts. These encouraging results call for further investigations in cellular models of oxidative stress, as this catalyst already possesses interesting properties. Overall, the rational approach adopted in this work led to a noticeable but weak improvement of the catalyst. This underlines the fact that designing a peptidyl sequence that is able to accommodate two metal centers and lead to complexes with the expected properties is not straightforward. Combining a combinatorial approach with activity-based screening may be a more valuable strategy in this case. Works in this direction are currently in progress.

4. Experimental Section

Peptide synthesis. Peptide synthesis was conducted by SPPS using Fmoc-Rink Amide MBHA (resin with a loading capacity of 0.53 mmol/g). Solid-phase peptide synthesis was performed manually with standard Fmoc-protected amino acids. Resin beads at a concentration of 0.200 mmol were first swelled in dichloromethane (DCM). Standard peptide coupling procedures were used for all amino acid couplings: the amino acid (3

equiv./equiv. resin) with *N,N'*-diisopropylcarbodiimide (DIC; 3 equiv./equiv. resin) and *N*-hydroxybenotriazole (HOBt; 3 equiv./equiv. resin) in dimethylformamide (DMF, 4 mL) were mixed with the resin for 1 h at room temperature under agitation. After each amino acid coupling, solvents and soluble reagents were removed under vacuum, and the resin was washed five times with DMF. Completion of the reaction was monitored by the Kaiser test, which indicates the presence of free amine by the deep blue coloration of the bead. Standard deprotection conditions of the Fmoc group were employed (20% piperidine in *N*-methyl-2-pyrrolidone (NMP) for 1 min under agitation and again for 15 min under agitation at room temperature), followed by washings with DMF. Final acetylation was performed with a solution of acetic anhydride in dichloromethane DCM (4 mL, 10/90, *v:v*) for 1 h at room temperature. Solvents and soluble reagents were removed by filtration. The resin was successively washed with DCM (5×4 mL) and then methanol (3×4 mL) and dried under vacuum for 1 h. Simultaneous lateral chain deprotection and bead cleavage were performed using a solution of TFA/H₂O/Trisopropylsilane (95%/2.5%/2.5%; 4 mL) (TFA, trifluoroacetic acid) for 2 h at room temperature. The samples became red/orange. The solution was collected by filtration in a 50 mL round-bottom flask, and beads were washed three times with neat TFA (3×3 mL). The TFA solutions were combined, and TFA was removed under reduced pressure. The crude solid was precipitated in cold diethyl ether and recovered by centrifugation (7000 rpm, 4 min). The solid was washed two more times with Et₂O. The peptide was dissolved in 20 mL of deionized H₂O and freeze-dried. The peptide was purified by reverse-phase HPLC using a linear gradient from 5 to 30% acetonitrile in a water bath containing 0.1% TFA for 30 min. High purity (>95%) was confirmed by analytical HPLC, and the expected mass was found by MALDI-TOF mass spectrometry. The list of the synthesized peptides is provided in Table S1.

Peptide stock solution preparation. The concentration of purified and lyophilized peptide dissolved in milliQ water was determined by measuring the absorbance of a diluted solution (5 μ L in 995 μ L of milliQ water) at 280 nm and by using the extinction coefficient of tyrosine ($1280 \text{ cm}^{-1}\text{M}^{-1}$).

Association constant measurement by fluorescence spectrometry. Cu(OAc)₂·H₂O was titrated into CAT_mx ($x = 1-5$) peptide solution in MOPS buffer (50 mM, pH 7.5) at 25 °C. After each addition of Cu(II), the emission spectrum (average of 2 accumulations) upon excitation at 275 nm was recorded between 280 and 400 nm ($\text{slit}_{\text{exc}} = \text{slit}_{\text{em}} = 5$ nm; scan rate = 200 nm/min). Before recording each spectrum, it was ensured that thermodynamic equilibrium was reached (stable fluorescence intensity). The intensity at the maximum of tyrosine emission (303 nm) was used to generate titration curves, which were then fitted using HypSpec software. HypSpec determines cumulative (β) binding constants for the first (β_1) and second (β_2) Cu(II) bindings to the peptide. From these cumulative binding constants, stepwise binding constants for the first (K_1) and second (K_2) Cu(II) bound to the peptide were determined. The provided K_d values are the average of two to three independent titrations \pm standard error of the mean (SEM).

Kinetic study of complex degradation by UV-visible spectroscopy. Complex (CAT_mx:Cu 1:2) degradation kinetics was monitored for each complex ($x = 1-5$) at 4 different concentrations (20, 50, 100 and 200 μ M) in MOPS buffer (50 mM, pH 7.5). The absorbance was recorded at 289 nm over time until a plateau was reached. The addition of H₂O₂ in excess (5 mM) to the cuvette corresponds to the beginning of the experiment (t_0). The initial rates of degradation product formation v_0 (taking into account their molar extinction coefficient (ϵ); see SI) were measured from the slope of the linear fit (from 0 to 30 s) for the different complex concentrations. For each complex concentration, measurements were performed twice, and the values used to plot Figure 3 are average \pm standard error of the mean (SEM). Then, k_{obs} corresponds to the slope of the linear fit of $v_0 = f([\text{complex}])$.

Catalytic activity. All measurements were carried out in MOPS buffer (50 mM, pH 7.5) at 25 °C in a micro-cell sealed with a rubber septum to avoid the introduction of O₂ from the air. The complex solution CAT_mx:Cu(OAc)₂ 1:2 ($x = 1-5$) at 100 μ M in MOPS was introduced into the micro-cell and sealed before being bubbled with dinitrogen gas to remove

dissolved dioxygen. H_2O_2 solution was then injected through the septum into the stirred complex solution. Reaction rates were determined by measuring the O_2 concentration evolution over time. The initial rates v_0 were determined from the slope of the linear fit (from 0 to 20 s) of dioxygen formation at several initial H_2O_2 concentrations (2.5, 5, 7.5, 10, 15, 20, 25 and 30 mM). The O_2 formation reaction from H_2O_2 exhibited Michaelis–Menten catalytic behavior, as is the case for the natural enzyme. Michaelis–Menten constants K_m , V_{\max} and k_{cat} were determined using the Lineweaver–Burk double reciprocal plot: $1/v_0 = f(1/[\text{H}_2\text{O}_2])$, in which the x-intercept corresponds to $-1/K_m$, the slope corresponds to K_m/V_{\max} and $V_{\max} = k_{\text{cat}}[\text{O}_2][\text{catalyst}]_0$. Since, during dismutation, two H_2O_2 molecules lead to the formation of a single O_2 molecule, $k_{\text{cat-disappearance H}_2\text{O}_2} = 2 \times k_{\text{cat-appearing O}_2}$. The TON was calculated as the maximum number of H_2O_2 moles consumed per mole of catalyst, $\text{TON} = 2[\text{O}_2]_{\text{max obs}}/[\text{catalyst}]_0$.

Supplementary Materials: The following supporting information can be downloaded at: <https://www.mdpi.com/article/10.3390/molecules27175476/s1>, Figure S1: Characterization of the synthesized peptides; Table S1: Characterization of the newly synthesized peptide; Figure S2: $\text{Cu}(\text{OAc})_2 \cdot \text{H}_2\text{O}$ titration into CATmx peptide solution in MOPS buffer (50 mM, pH 7.5) at 25 °C; Table S2: Apparent association constants of the two binding sites for each complex measured using fluorescence spectroscopy at 25 °C in MOPS buffer (50 mM, pH 7.5); Figure S3: Circular dichroism spectra of CATmx (dashed lines) and CATmx:Cu 1:2 mixtures (solid lines) at 133 μM ($x = 1-5$); Figure S4: Subtracted UV-vis spectra (after - before addition of a large excess of H_2O_2) of CATmx:Cu 1:2 mixtures ($x = 1-5$); Figure S5: Dioxygen evolution monitored using a Clark-type electrode of CATmx:Cu 1:2 mixtures ($x = 1-5$) at 100 μM in MOPS buffer (50 mM, pH 7.5) at 25 °C in presence of increasing concentrations of $[\text{H}_2\text{O}_2]$ (from 2.5 mM to 30 mM). Figure S6. Molar extinction coefficient (\mathcal{E}) determination of the degradation product of CATmx:Cu(OAc)₂ 1:2 ($x = 1$ to 5). Excess H_2O_2 (50 mM) was added to initial solutions of complex at different concentrations (25, 50, 62.5, 100 and 125 μM) in MOPS (50 mM, pH 7.5). The absorbance at 289 nm of this solution was measured for the different concentrations and enabled the determination of \mathcal{E} . Reference [19] is cited in the supplementary materials.

Author Contributions: Conceptualization, C.P. and N.D.; methodology, C.P. and N.D.; validation, C.P. and N.D.; formal analysis, Y.B.H.H. and N.D.; investigation, Y.B.H.H., K.C., A.B., M.T.S.H. and N.D.; data curation, Y.B.H.H., K.C. and N.D.; writing—original draft preparation, Y.B.H.H.; writing—review and editing, Y.B.H.H., C.P. and N.D.; visualization, Y.B.H.H. and N.D.; supervision, N.D.; project administration, N.D.; funding acquisition, C.P. and N.D. All authors have read and agreed to the published version of the manuscript.

Funding: This research was funded by ANR JCJC MetalloPepZyme, ANR-16-CE07-0025, ANR MOBIDIC and ANR-21-CE18-0053-01.

Acknowledgments: The authors thank Thibaud Coradin (and the LCMCP) for his help with the circular dichroism experiments. We thank the IBPS SU, FR3631 mass spectrometry and peptide synthesis core facilities for access to the MALDI-TOF spectrometer and for providing us with peptides, respectively.

Conflicts of Interest: The authors declare no conflict of interest.

Sample Availability: Samples of the compounds are available from the authors.

References

1. Halliwell, B.; Gutteridge, J.M.C. Oxygen Toxicity, Oxygen Radicals, Transition Metals and Disease. *Biochem. J.* **1984**, *219*, 1–14. [[CrossRef](#)] [[PubMed](#)]
2. Auten, R.L.; Davis, J.M. Oxygen Toxicity and Reactive Oxygen Species: The Devil Is in the Details. *Pediatr. Res.* **2009**, *66*, 121–127. [[CrossRef](#)] [[PubMed](#)]
3. Murphy, M.P.; Holmgren, A.; Larsson, N.-G.; Halliwell, B.; Chang, C.J.; Kalyanaraman, B.; Rhee, S.G.; Thornalley, P.J.; Partridge, L.; Gems, D.; et al. Unraveling the Biological Roles of Reactive Oxygen Species. *Cell Metab.* **2011**, *13*, 361–366. [[CrossRef](#)] [[PubMed](#)]
4. Sies, H.; Berndt, C.; Jones, D.P. Oxidative Stress. *Annu. Rev. Biochem.* **2017**, *86*, 715–748. [[CrossRef](#)]
5. Sies, H.; Jones, D.P. Reactive Oxygen Species (ROS) as Pleiotropic Physiological Signalling Agents. *Nat. Rev. Mol. Cell Biol.* **2020**, *21*, 363–383. [[CrossRef](#)]

6. McCord, J.M.; Edeas, M.A. SOD, Oxidative Stress and Human Pathologies: A Brief History and a Future Vision. *Biomed. Pharmacoter.* **2005**, *59*, 139–142. [[CrossRef](#)]
7. Sheng, Y.; Abreu, I.A.; Cabelli, D.E.; Maroney, M.J.; Miller, A.-F.; Teixeira, M.; Valentine, J.S. Superoxide Dismutases and Superoxide Reductases. *Chem. Rev.* **2014**, *114*, 3854–3918. [[CrossRef](#)]
8. Wang, Y.; Branicky, R.; Noë, A.; Hekimi, S. Superoxide Dismutases: Dual Roles in Controlling ROS Damage and Regulating ROS Signaling. *J. Cell. Biol.* **2018**, *217*, 1915–1928. [[CrossRef](#)]
9. Veal, E.A.; Day, A.M.; Morgan, B.A. Hydrogen Peroxide Sensing and Signaling. *Mol. Cell* **2007**, *26*, 1–14. [[CrossRef](#)]
10. Winterbourn, C.C. Biological Production, Detection, and Fate of Hydrogen Peroxide. *Antioxid. Redox Signal.* **2018**, *29*, 541–551. [[CrossRef](#)]
11. Gardner, P.R.; Raineri, I.; Epstein, L.B.; White, C.W. Superoxide Radical and Iron Modulate Aconitase Activity in Mammalian Cells*. *J. Biol. Chem.* **1995**, *270*, 13399–13405. [[CrossRef](#)]
12. Halliwell, B.; Gutteridge, J.M.C. *Free Radicals in Biology and Medicine*, 5th ed.; Oxford University Press: New York, NY, USA, 2015; ISBN 978-0-19-871748-5.
13. Salvemini, D.; Muscoli, C.; Riley, D.P.; Cuzzocrea, S. Superoxide Dismutase Mimetics. *Pulm. Pharmacol. Ther.* **2002**, *15*, 439–447. [[CrossRef](#)]
14. Batinic-Haberle, I.; Tovmasyan, A.; Roberts, E.R.H.; Vujaskovic, Z.; Leong, K.W.; Spasojevic, I. SOD Therapeutics: Latest Insights into Their Structure-Activity Relationships and Impact on the Cellular Redox-Based Signaling Pathways. *Antioxid Redox Signal.* **2014**, *20*, 2372–2415. [[CrossRef](#)]
15. Vincent, A.; Thauvin, M.; Quévrain, E.; Mathieu, E.; Layani, S.; Seksik, P.; Batinic-Haberle, I.; Vriza, S.; Policar, C.; Delsuc, N. Evaluation of the Compounds Commonly Known as Superoxide Dismutase and Catalase Mimics in Cellular Models. *J. Inorg. Biochem.* **2021**, *219*, 111431. [[CrossRef](#)]
16. Policar, C.; Bouvet, J.; Bertrand, H.C.; Delsuc, N. SOD Mimics: From the Tool Box of the Chemists to Cellular Studies. *Curr. Opin. Chem. Biol.* **2022**, *67*, 102109. [[CrossRef](#)]
17. Signorella, S.; Hureau, C. Bioinspired Functional Mimics of the Manganese Catalases. *Coord. Chem. Rev.* **2012**, *256*, 1229–1245. [[CrossRef](#)]
18. Tovmasyan, A.; Maia, C.G.C.; Weitner, T.; Carballal, S.; Sampaio, R.S.; Lieb, D.; Ghazaryan, R.; Ivanovic-Burmazovic, I.; Ferrer-Sueta, G.; Radi, R.; et al. A Comprehensive Evaluation of Catalase-like Activity of Different Classes of Redox-Active Therapeutics. *Free Radic. Biol. Med.* **2015**, *86*, 308–321. [[CrossRef](#)]
19. Coulibaly, K.; Thauvin, M.; Melenbacher, A.; Testard, C.; Trigoni, E.; Vincent, A.; Stillman, M.J.; Vriza, S.; Policar, C.; Delsuc, N. A Di-Copper Peptidyl Complex Mimics the Activity of Catalase, a Key Antioxidant Metalloenzyme. *Inorg. Chem.* **2021**, *60*, 9309–9319. [[CrossRef](#)]
20. Kirkman, H.N.; Gaetani, G.F. Mammalian Catalase: A Venerable Enzyme with New Mysteries. *Trends Biochem. Sci.* **2007**, *32*, 44–50. [[CrossRef](#)]
21. Whittaker, J.W. Non-Heme Manganese Catalase—The ‘Other’ Catalase. *Arch. Biochem. Biophys.* **2012**, *525*, 111–120. [[CrossRef](#)]
22. Barynin, V.V.; Whittaker, M.M.; Antonyuk, S.V.; Lamzin, V.S.; Harrison, P.M.; Artymiuk, P.J.; Whittaker, J.W. Crystal Structure of Manganese Catalase from *Lactobacillus Plantarum*. *Structure* **2001**, *9*, 725–738. [[CrossRef](#)]
23. Day, B.J. Catalase and Glutathione Peroxidase Mimics. *Biochem. Pharmacol.* **2009**, *77*, 285–296. [[CrossRef](#)] [[PubMed](#)]
24. Singh, R.; Haukka, M.; McKenzie, C.J.; Nordlander, E. High Turnover Catalase Activity of a Mixed-Valence MnII/MnIII Complex with Terminal Carboxylate Donors. *Eur. J. Inorg. Chem.* **2018**, *2015*, 3485–3492. [[CrossRef](#)]
25. Mu, J.; Zhang, L.; Zhao, M.; Wang, Y. Co₃O₄ Nanoparticles as an Efficient Catalase Mimic: Properties, Mechanism and Its Electrocatalytic Sensing Application for Hydrogen Peroxide. *J. Mol. Cat. A Chem.* **2013**, *378*, 30–37. [[CrossRef](#)]
26. Zhou, J.; Chen, Y.; Lan, L.; Zhang, C.; Pan, M.; Wang, Y.; Han, B.; Wang, Z.; Jiao, J.; Chen, Q. A Novel Catalase Mimicking Nanocomposite of Mn(II)-Poly-L-Histidine-Carboxylated Multi Walled Carbon Nanotubes and the Application to Hydrogen Peroxide Sensing. *Anal. Biochem.* **2019**, *567*, 51–62. [[CrossRef](#)] [[PubMed](#)]
27. Gao, J.; Martell, A.E.; Reibenspies, J.H. Novel Dicopper(II) Catalase-like Model Complexes: Synthesis, Crystal Structure, Properties and Kinetic Studies. *Inorg. Chim. Acta* **2003**, *346*, 32–42. [[CrossRef](#)]
28. Kaizer, J.; Csonka, R.; Speier, G.; Giorgi, M.; Réglie, M. Synthesis, Structure and Catalase-like Activity of New Dicopper(II) Complexes with Phenylglyoxylate and Benzoate Ligands. *J. Mol. Cat. A Chem.* **2005**, *236*, 12–17. [[CrossRef](#)]
29. Kaizer, J.; Csay, T.; Speier, G.; Réglie, M.; Giorgi, M. Synthesis, Structure and Catalase-like Activity of Cu(N-Baa)₂(Phen) (Phen = 1,10-Phenanthroline, N-BaaH = N-Benzoylanthranilic Acid). *Inorg. Chem. Commun.* **2006**, *9*, 1037–1039. [[CrossRef](#)]
30. Ramadan, A.E.-M.M. Syntheses and Characterization of New Tetraazamacrocyclic Copper(II) Complexes as a Dual Functional Mimic Enzyme (Catalase and Superoxide Dismutase). *J. Coord. Chem.* **2012**, *65*, 1417–1433. [[CrossRef](#)]
31. Pires, B.M.; Silva, D.M.; Visentin, L.C.; Rodrigues, B.L.; Carvalho, N.M.F.; Faria, R.B. Synthesis and Characterization of Cobalt(III), Nickel(II) and Copper(II) Mononuclear Complexes with the Ligand 1,3-Bis[(2-Aminoethyl)Amino]-2-Propanol and Their Catalase-Like Activity. *PLoS ONE* **2015**, *10*, e0137926. [[CrossRef](#)]
32. Richezzi, M.; Ferreyra, J.; Puzzolo, J.; Milesi, L.; Palopoli, C.M.; Moreno, D.M.; Hureau, C.; Signorella, S.R. Versatile Activity of a Copper(II) Complex Bearing a N4-Tetradentate Schiff Base Ligand with Reduced Oxygen Species. *Eur. J. Inorg. Chem.* **2022**, *2022*, e202101042. [[CrossRef](#)]

33. Krieger, F.; Möglich, A.; Kiefhaber, T. Effect of Proline and Glycine Residues on Dynamics and Barriers of Loop Formation in Polypeptide Chains. *J. Am. Chem. Soc.* **2005**, *127*, 3346–3352. [[CrossRef](#)]
34. Hureau, C.; Faller, P. A β -Mediated ROS Production by Cu Ions: Structural Insights, Mechanisms and Relevance to Alzheimer's Disease. *Biochimie* **2009**, *91*, 1212–1217. [[CrossRef](#)]
35. Pires dos Santos, M.L.; Faljoni-Alário, A.; Mangrich, A.S.; Costa Ferreira, A.M. da Antioxidant and Pro-Oxidant Properties of Some Di-Schiff Base Copper(II) Complexes. *J. Inorg. Biochem.* **1998**, *71*, 71–78. [[CrossRef](#)]
36. Tang, Q.; Wu, J.-Q.; Li, H.-Y.; Feng, Y.-F.; Zhang, Z.; Liang, Y.-N. Dinuclear Cu(II) Complexes Based on p-Xylylene-Bridged Bis(1,4,7-Triazacyclononane) Ligands: Synthesis, Characterization, DNA Cleavage Abilities and Evaluation of Superoxide Dismutase- and Catalase-like Activities. *Appl. Organomet. Chem.* **2018**, *32*, e4297. [[CrossRef](#)]
37. Guerreiro, J.F.; Gomes, M.A.G.B.; Pagliari, F.; Jansen, J.; Marafioti, M.G.; Nistico, C.; Hanley, R.; Costa, R.O.; Ferreira, S.S.; Mendes, F.; et al. Iron and Copper Complexes with Antioxidant Activity as Inhibitors of the Metastatic Potential of Glioma Cells. *RSC Adv.* **2020**, *10*, 12699–12710. [[CrossRef](#)]
38. Shank, M.; Barynin, V.; Dismukes, G.C. Protein Coordination to Manganese Determines the High Catalytic Rate of Dimanganese Catalases. Comparison to Functional Catalase Mimics. *Biochemistry* **2002**, *33*, 15433–15436. [[CrossRef](#)]